Fluid Inclusion Analysis as Additional Tool for Comprehension of Petroleum Systems: A Case Study from the Pannonian Basin (Hungary)*

Barbara Szabó[1], Felix Schubert[2], Herbert Volk[3], and Manzur Ahmed[3]

Search and Discovery Article #40917 (2012)
Posted April 23, 2012

*Adapted from extended abstract prepared in conjunction with poster presentation at AAPG Annual Convention and Exhibition, Long Beach, California, April 22-25, 2012, AAPG©2012

[1]Exploration and Production, MOL Plc., Budapest, Hungary (barbokster@gmail.com)
[2]Department of Mineralogy Geochemistry and Petrology, University of Szeged, Szeged, Hungary
[3]Petroleum Systems, CSIRO Earth Science and Resource Engineering, North Ryde, NSW, Australia

Abstract

The successful exploration and appraisal of a field requires deep insight into the petroleum system of the given basin. Fluid inclusion petrography and microthermometry combined with the geochemical analysis of source rock extracts, crude oil, and the petroleum trapped within fluid inclusions by Molecular Composition of Inclusions (MCI) procedures offer additional information about the petroleum system. The case study from the Pannonian Basin represents the use of fluid inclusions as the witnesses of geological and geochemical processes in a fractured reservoir and the adjacent sedimentary basin.

In the study area, fractures in volcanic carrier beds and reservoir rocks were cemented by different minerals, in particular by zeolites. Based on fracture-filling mineral sequences as well as their textural relationships, four distinct vein types can be distinguished, but only the youngest one preserves the migrated hydrocarbon-bearing fluid trapped in zeolites (analcime, heulandite) and allows oil to accumulate in a reservoir scale. Petrographically, two different petroleum inclusion assemblages could be distinguished. The very infrequent, single primary HC1 inclusions with weak yellow fluorescence colour were trapped earlier than the abundant primary HC2 inclusions with intense blue fluorescence colour. The UV-fluorescence micro-spectroscopy strengthened the distinction of the two different types and established the similarity of crude oil produced in the area and late (HC2) fluid inclusion oil. Based on the homogenization temperatures of the primary aqueous inclusions co-genetic with HC2 petroleum-bearing inclusions, the migration of the HC2 fluid in the fracture system took place in the temperature range of 130-160 °C. Molecular composition of the fluid inclusion oil was correlated with rock extracts of representative source rock samples (MS1, MS2) and crude oil produced in the area. The

biomarker signatures of the fluid inclusion oil and the crude oil are very similar to each other. The crude oil looks unbiodegraded, akin to MS2 rock extract. Both oils appear to represent a marine (carbonate) influenced source facies but deposited in a slightly more anoxic environment than the source rock samples derived, probably from a deeper part of the basin. The results confirm that fluid inclusion measurements could be used as effective exploration tools for comprehension of the petroleum system in the area.

Introduction

The successful exploration for petroleum and the appraisal of a field requires detailed insights into the petroleum systems of the exploration area. Even at the production phase of a field it may be difficult to build charge history models and pinpoint effective source rocks and their thermal maturities. Geochemical analysis of production oil (PO) and solvent extracts of potential source rocks can provide important information. However, the composition of petroleum in the reservoir may be a result of a complex charge history. Oils are often trapped in fluid inclusions in or near the oil field, and the study analysis of these fluid inclusion oils (FIO) offers an opportunity to gain insights into fluid properties of the oil field in the past. The aims of this study were to understand the filling history of the Üllés Field in the southern part of the Pannonian Basin in Hungary by using fluid inclusion petrography, microthermometry, ultraviolet (UV) microspectroscopy, and geochemical analysis of source rock extracts, PO and FIO.

Geological Setting

Extensive Miocene volcanic activity produced thick basaltic and pyroclastic successions that can be traced across the central and western part of the Great Hungarian Plain. The Kecel Basalt Formation was deposited during this activity, and hosts the Üllés Field (Figure 1), which was discovered in 1980. As a result of periodic submarine eruptions, volcanic rocks of this formation are intercalated with thick layers of Endrőd Marl Formation which reaches up to several hundreds of meters. The Endrőd Marl is regarded as one of the most important source rock in the area, although in many areas its thermal maturity is highly variable and oil-source correlations are not unequivocal (e.g. Badics et al., 2011; Badics and Veto, 2012 and references therein). The lithofacies of the Endrőd Marl varies from calcareous to argillaceous marls, depending on palaeo water depth and other depositional conditions in the Lake Pannon, a large, long-lived, brackish water body filling the Pannonian Basin from the end of the Middle Miocene to the Early Pliocene (Magyat et al., 1999).

The Late Miocene Kecel Basalt Formation hosting petroleum in fractures were penetrated by 11 wells in the region of the Üllés Field between 2200 and 2700 meters, and basalts in its fractured reservoir show intense chloritization and carbonatization as the result of metasomatism following the subaqueous volcanism. Fractures are often cemented by minerals (prehnite, chlorite, quartz, calcite), in particular by different zeolites (laumontite, thomsonite, analcime, mesolite, heulandite, stilbite) (Szabo et al., 2009). Four distinct vein types can be distinguished based on textural relationships of mineral sequences. The subservient veins of the earliest K-

feldspar (Kfp)-type could be found only in lapillis and contain potassium feldspar, quartz, albite, laumontite, and calcite. The basalt hosted Calcite (Cal)-type veins are filled by altered volcanic material, calcite, and heulandite. These types formed prior to significant diagenetic alteration of the pyroclastic material. The Laumontite (Lmt)-type veins formed later, during the formation of the early fracture network and are composed of prehnite-laumontite-thomsonite-laumontite-chlorite-calcite phases. The infrequent Analcime (Anl)-type consists of analcime, mesolite, heulandite and stilbite, and could be related to a later fracture generation. Only the youngest generation of veins (the dominantly analcime containing Anl-type) preserved hydrocarbon-bearing fluids (Szabo et al., 2009). Petroleum inclusions were trapped in analcime and heulandite crystals within the Anl-type veins. Details on these fracture fillings can be found in Szabo et al., 2009.

Samples and Methods

Fluid inclusion petrography and microthermometry were performed on thin sections made from core samples of Üllés-61 well and cuttings of Üllés-65A well. For geochemical analysis solvent extracts of two source rock samples (Marl S1 and Marl S2), one PO and one FIO were used. Both oils are from Üllés-61 well, the FIO is from the fracture-filling analcime cement and the PO was sampled from the well head.

Prior to the analytical procedures double-polished thick sections (75-150 μm) were prepared from the cores and cuttings, and where necessary, the samples were impregnated by epoxy resin under vacuum at 40 °C for a t least 24 hours. The preparation of thick sections followed the instructions of Shepherd et al., 1985. The sections were then examined to classify fluid inclusion assemblages following the criteria of Goldstein and Reynolds 1994.

Microthermometry was carried out using a Linkam THMSG-600 heating-freezing stage mounted on an Olympus BX41 microscope using LWD objectives with 40x and 100x magnification. The stage was calibrated using synthetic fluid inclusions trapped in quartz at -56.6, 0.0 and 374 °C. The microthermometric results are accurate with in ±0.2 °C at T<100 °C, and within ±0.5 °C at 100< T<150 °C. The homogenization temperature (Th) was usually determined by the cycling method (Goldstein and Reynolds 1994). The salinities of the aqueous inclusions were calculated from the final ice melting temperatures (T_m(Ice)) and reported in mass% of NaCl equivalent (Bodnar 1993). The concentrations of methane in the methane-bearing inclusions were not known, so the possible effects of the dissolved methane and the methane-hydrate-clathrate to the salinity estimation could not be accounted for. The salinities reported in the present study are therefore maximum values (Schubert et al., 2007).

Based on the petrographic evaluation of the thick sections UV fluorescent micro-spectroscopic measurements were carried out to identify the different petroleum inclusion assemblages. For this purpose a PARISSH Spectral Imaging System (Lightform Inc., Hillsborough, NJ, USA) mounted on an Olympus IX71 inverted research microscope was used to collect the fluorescence spectra.

The light from a selected line of the microscope's field of view is wavelength dispersed by the spectrometer and focused on a Peltier-cooled charge coupled device. The recorded image consists of intensity values with their spatial and wavelength coordinates. The spectral imaging system provides simultaneously several full spectra uniformly distributed along a conveniently selected spatial direction. In these investigations the observation line (projection of the entrance slit) was chosen to be through the entire inclusion. During the detection we used an Olympus U-MSWB2 filter cube (excitation filter - 420-480 nm, emission filter - 520IF, dichromatic mirror - 500 nm). During the measurement we collected ca. 100 spectra on each hydrocarbon containing inclusion. To optimize the signal-to-noise ratios we chose the spectrum of the highest intensity among the collected spectra of the single petroleum inclusions.

Based on the petrographic analysis, one core sample containing the youngest vein type was selected for detailed geochemical analysis of oil trapped in analcime-hosted fluid inclusions. The selected core sample was mechanically disintegrated and the analcime grains from the veins were separated from the host rock and the other minerals. FIO from the analcime grains were analyzed according to the molecular composition of inclusions (MCI) protocols outlined in George et al., 2007. Potential surface contaminations of the crystals were removed by successive rinsing with organic solvents of different polarities, that were monitored by gas chromatography - mass spectrometry (GC-MS) analysis of outside-rinse and system blanks. Analcime crystals were crushed under solvent (dichloromethane) using the off-line method (crush-leach in a mill under atmospheric pressure), and on-line in an MSSV-II thermal extraction port for the analysis of light hydrocarbons. An AutoSpecQ GC-MS system was used for both on- and off-line analyses of the FIO, and ionization products were recorded using single ion monitoring (SIM) and metastable reaction monitoring (MRM) experiments. Details on instrumental settings are provided in George et al., 2007. Aliphatic and aromatic hydrocarbon fractions of the U61 PO were analysed using magnet scan (*m/z* 50-550), SIM and MRM experiments. The distribution of light hydrocarbons in the U61 PO was determined using two complementary GC runs with flame ionization detection following a modified method of George et al., 2002.

Results

FI petrography, microthermometry, and UV fluorescent petrography

The youngest of the four vein types - the Anl-type - preserves the migrated hydrocarbon-bearing fluid trapped as fluid inclusions, which could be studied in detail in the cores of the Üllés-61 well. The dense fracture network in the basaltic and pyroclastic rock is partly or completely filled by zeolites (mesolite, analcime, heulandite and stilbite). The dominant fracture-filling mineral is analcime and its transparent or whitish, leucitohedron crystals could be well identified in the partly opened fractures and voids. White, layered heulandite crystals could be observed on the analcime crystals. The tiny needles of mesolite appear as solid inclusions scattered in the analcime and as thick clusters in heulandite. The massive, milky stilbite appears just at places and seems to not contain any

inclusion. The mineral sequence of this vein type is analcime±mesolite →heulandite±mesolite →stilbite. Based on optical observations and Raman spectroscopy performed on cuttings, the presence of the same vein type in the Üllés-65/A well is assumed.

In Anl-type veins only the analcime and the heulandite contain fluid inclusions. An early and a late primary (P) aqueous (AQ) fluid inclusion assemblages could be distinguished (AQ_P1 and AQ_P2) in analcime, consisting of irregularly shaped inclusions with a size up to 65 µm (Ü-65A). The primary aqueous inclusions in analcime consist of saline water and small methane bubbles with an invariant gas and liquid range $_{(\phi vap)}$ at room temperature.

Petrographically, two different hydrocarbon (HC) inclusion assemblages could be distinguished. The very infrequent primary HC1_P inclusions were trapped prior to the AQ_P2 late primary aqueous inclusions. These irregular, two-phase inclusions show a low intensity, yellow fluorescence color under UV excitation. The primary HC2 inclusions have intense blue fluorescence color and they could be observed along several succeeding growth zones. At least five zones could be distinguished in Üllés-61 (HC2_P1, HC2_P2, HC2_P3, HC2_P4, HC2_P5). Sometimes three-phase, oil-bearing aqueous inclusions occur in the zone of AQ_P2 or HC2_P1, which proves that the HC2 inclusions of the earliest zone (HC2_P1) are co-genetic with the AQ_P2 inclusions. The shapes of HC2 inclusions are more rounded than the aqueous inclusions, and their sizes are up to 75 µm in Ü-65A. The volume fraction of the vapour phase $_{(\phi vap)}$ in the HC2 inclusions is mostly uniform at room temperature.

UV-fluorescence micro-spectroscopy confirms that the two different FIO types trapped different oil types, and indicate that the crude oil produced in the field is more similar to the oil trapped in the later formed HC2 fluid inclusion assemblage (Figure 2). API gravities estimated from fluorescence color are 30-35°, for HC1 and 40-45° for HC2 when following the approach outlined in Bodnar 1990.

Results of microthermometric measurements are provided in Table 1 and in Figure 3 for AQ_P2 and HC2_P1 inclusions. Inclusions of the two aqueous inclusion assemblages undergo homogenization to liquid $_{(LAQ+V\rightarrow LAQ)}$ 124 to 132 °C (AQ_P1 inclusions) and at 129 to 149 ºC (in Üllés-61) and 131 to 142 ºC (in Üllés-65A) (both AQ_P2). Based on the T_m(Ice) value of -0.3 ºC, the calculated salt content of the AQ_P2 inclusions is ca. 0.53 mass% in NaCl equivalent (Bodnar 1993). The T_h of HC1_P inclusions were very hard to measure, since inclusions generally decrepitated before the homogenization. However, one successful measurement yielded a T_h of 121.5 ºC. HC2 inclusions were trapped along (at least) five different growth zones in Üllés-61, but their homogenization do not show any appreciable temperature variance. The T_h into the liquid phase were as follows for the subsequent zones of HC inclusions HC2_P1: 108-136 ºC, HC2_P2: 110-125 ºC, HC2_P3: 110-126 ºC, HC2_P4: 114-123 ºC, HC2_P5: 111-120 ºC in Üllés-61. The primary HC2 inclusions (co-genetic with the aqueous inclusions) homogenize between 108-118 ºC in Üllés-65A.

The AQ_P2 and HC2_P1 inclusions have more similar T_h in Üllés-61 than AQ_P2 and HC2 inclusions in Üllés-65A, which refers to trapping of more gas-saturated phases (Tseng and Pottorf 2002) (Figure 3).

The properties of the trapped oil can be estimated from microthermometric measurements at low temperatures (Grimmer et al., 2003). Both the HC1 and the HC2 containing inclusions are in the two-phase domain at room temperature, and they homogenize into the liquid phase. Below 20 ºC, HC2 containing inclusions have solids in the liquid phase, and while heating the cooled sample, the slight movements of these particles could be observed with the form changes of the vapour bubble. HC1 inclusions do not show any of these reactions at low temperatures. According to Grimmer et al., 2003 HC1_P inclusions show the behavior of inclusions containing black oil, and HC2_P inclusions act like they contain light oil (Figure 4).

Geochemistry

The molecular composition of Üllés-61 FIO was compared to extracts of representative source rock samples (Marl S1 and Marl S2) and to PO produced from the same well. The MCI data represents dominantly the HC2 fluid inclusion assemblage, since HC1 inclusions are very rare in this sample (Figure 2). Üllés-61 FIO yielded 44 µg of *n*-alkanes in the range of *n*-C_{12-32} per g of sample, and is the richest fluid inclusion oil analysed in CSIRO's laboratory to date. Extraction yields from final outside rinse and procedural laboratory system blanks are orders of magnitudes lower than the yield of FIO oil, and hence the MCI data can be can be interpreted with great confidence. Selected geochemical parameters are provided in Table 2.

The *n*-alkane profiles of the 4 samples are shown in Figure 5. None of samples appear to be affected by biodegradation, as indicated by the presence of abundant *n*-alkanes and the absence of humps of unresolved complex mixtures. The light hydrocarbon distributions of both the PO and the FIO are very similar and typical for unbiodegraded mature oils with a moderate aromatic content.

The *n*-alkanes in Marl S1 show a bimodal distribution, with a first maximum at *n*-C_{15} and a second maximum at *n*-C_{27}. The *n*-alkanes in Marl S2 extract, FIO and PO show unimodal distributions with maxima at *n*-C_{17} (Marl S2 extract) and *n*-C_{16} (FIO and PO). *n*-Alkanes of the dominant range are likely to be derived from aquatic organic matter, whereas the high molecular weight *n*-alkanes (*n*-C_{23+}) are typically due to input from land plant waxes. *n*-Alkanes of Marl 1 extract with carbon numbers between 23 and 33 show a pronounced odd-over-even predominance (CPI 26-32 =1.18), pointing to contributions of terrestrial plant waxes at low to moderate thermal maturities. A slight odd-over-even *n*-alkane predominance in this molecular weight range is also apparent for the oils, suggesting some terrestrial plant input to their source rocks. No such predominance can be seen for Marl S2 extract.

The pristane/phytane (Pr/Ph) ratio of Marl S1 extract is 2.8, much higher than the Pr/Ph ratios for the Marl S2 extract (1.10) and the FIO and PO (ca. 0.7). This suggests a reducing depositional environment for the Marl S2 sample, and an even more reducing character for the source rocks of FIO and PO, while Marl 1 was probably deposited in a more oxic environment. The other aliphatic biomarkers suggest that the FIO and PO are very similar and more closely related to Marl S2 than to Marl S1 extract. Hopanes are dominated by the C_{30} αβ homologue, with C_{29} αβ/C_{30} αβ hopane ratios ranging from 0.44 to 0.47 for FIO, PO and Marl S2 extract, and a significantly higher value for the Marl S1 extract (0.66). Both oils and the Marl S2 feature a prominent peak due to oleanane ± lupane and also peaks due to A-ring angiosperm (dO and dU), while these compounds are absent in the Marl S1 extract (Figure 6).

This suggests input from Cretaceous or younger angiosperm flowering plants to the Marl S2 and also to the source rocks of the oils. The presence of extended tricyclic terpanes is also restricted to the FIO, PO and Marl S2 extract (ETR = 0.70 – 1.00, Table 2), while the Marl S1 extract has a much higher abundance of C_{24} tetracyclic terpane compared to C_{23} tricyclic terpanes (C_{24} tetracyclic/C_{23} tricyclic terpane ratios = 2.4, Table 2, Figure 6) and C_{26} tricyclic terpanes (C_{24} tetracyclic/C_{26} tricyclic terpanes ratio = 1.06 Table 2). Gammacerane is a significant peak in all samples but least abundant in the Marl S2 extract (Gammacerane/C_{30} αβ hopane ratios, Table 2, Figure 6).

The relative abundance of diahopanes and other re-arranged terpanes is low in all samples, indicating that clays providing catalytic sites for structural re-arrangement are not abundant in the marls and in the source rocks of the oils. The relative abundance of C_{29} steranes to C_{29} hopanes is highest in the oils, about half as high in Marl S2 extract and an order of magnitude lower in the Marl S1 extract (Table 2). This may reflect a greater input from terrestrial plants for the FIO, PO and Marl S2 extract. *n*-Propylcholestanes, markers for marine chrysophyte algae, could be detected in all samples except in Marl S1 extract. This, together with a C_{26}/C_{25} tricyclic terpane ratio above unity (Schiefelbein 1999) may indicate a lacustrine depositional environment for the Marl S1 extract (Table 2, Figure 6). The age-specific abundance of C_{26} 24-nordiacholestanes and 24-norcholestanes is high to very high when compared to reference oils described in Holba et al., 1998, and hence consistent with the Cenozoic age and origin of the sediments and oils (Table 2). C_{29} steranes relative to C_{27} steranes are more abundant in the Marl S2 extracts and the oils, suggesting a greater input from terrestrial plants to these sediments and oils (Table 2) consistent with higher sterane to hopane ratios.

The higher relative abundance of moretanes compared to hopanes in the Marl S1 extract suggests its least maturity, which is consistent with its relatively low Ts/Tm ratio (Table 2, Figure 6) and sterane maturity parameters (e.g. C_{29} ααα S/(S+R), C_{29} αββ/(αββ+ααα) Table 2). When using a correlation published in Sofer et al., 1993 the C_{29} S/R ααα isomerization points to vitrinite reflectance equivalents (VRE) of 0.7% for Marl S1 and 0.80 - 0.84% for FIO, PO and Marl S2 extract.

All oils and rock extracts have low sulfur contents, with dibenzothiophene (DBT)/phenanthrene ratios between 0.07 and 0.17 (Table 2). The sulfur content of the oils is greater than the sulfur content of the marl extracts. Hughes et al., 1995 suggested a cross plot of

DBT/phenanthrene versus Pr/Ph to differentiate oils derived from various depositional environments. When applying their criteria for source rock differentiation the two marl samples plot in Zone 3 (marine and lacustrine) and the two oils in Zone 2 (lacustrine, sulfate-poor). However, aliphatic biomarkers only point to a lacustrine environment for Marl S1

A range of parameters based on aromatic hydrocarbons suggests that the Marl S1 extract is the least mature sample, and that the FIO is slightly less thermally mature than the PO. The calculated maturities obtained from MPI-1 (R_c = 0.74- 0.79%) are similar to the VRE values (0.70 –0.84%) derived from sterane isomerization (Table 2), and point to an early to peak oil window maturity for all samples.

Conclusions

- Based on the visual UV fluorescence colors (HC1-Yellow, HC2-Blue) and the λ_{max} values of UV fluorescence spectra (HC1-585 nm, HC2-548 nm), the API gravity of the HC1 oil is estimated to be around 30-35°, and the API gravity of the HC2 oil to be around 40-45°.
- Based on the T_h of the primary aqueous inclusions co-genetic with HC2 petroleum-bearing inclusions, the migration of the HC2 fluid in the fracture system took place in a temperature range of 130-160 °C.
- Based on the abundance of HC1 and HC2 the geochemical composition of the FIO largely reflects the younger fluid inclusion assemblage HC2.
- Both the FI oil and the production oil do not show any indications for biodegradation
- Aliphatic biomarkers suggest that the FIO and PO are very similar and are more closely related to Marl S2 than to Marl S1 extract.
- The oils were probably derived from the same source rock containing predominantly terrestrial organic matter with some marine inputs, deposited in anoxic conditions. Only Marl S1 has a signature, which may be classified as lacustrine. However, signatures in oils and sediments connected to the large Lake Pannon may be atypical due to its size and brackish environment.
- The Marl S1 sample is the least thermally mature sample, and has a maturity in the early oil window. The oils and the Marl S2 are slightly more mature and may have reached peak oil window maturities.

Acknowledgement

We thank David Fuentes (CSIRO Earth Science and Resource Engineering) for help with on-line FIO analyses and are grateful to MOL Plc. for providing the core samples, cuttings and the production oil.

References

Badics, B., and I. Vetö, 2012, Source rocks and petroleum systems in the Hungarian part of the Pannonian Basin: The potential for shale gas and shale oil plays: Marine and Petroleum Geology, v. 31, p. 53-69.

Badics, B., A. Uhrin, I. Vetö, A. Bartha, and C. Sajgo, 2011, Basin-centred gas in the Makó Trough, Hungary: a 3D basin and petroleum system modelling investigation: Petroleum Geoscience, v. 17, p. 405-416.

Bodnar, R.J., 1990, Petroleum migration in the Miocene Monterey Formation, California, USA: constraints from fluid-inclusion studies: Mineralogical Magazine, v. 54, p. 295-304.

Bodnar, R.J., 1993, Revised equation and table for determining the freezing point depression of H_2O-NaCl solutions: Geochimica et Cosmochimica Acta, v. 57, p. 683-684.

George, S.C., C.J. Boreham, S.A. Minifie, and S.C. Teerman, 2002, The effect of minor to moderate biodegradation on C_5 to C_9 hydrocarbons in crude oils: Organic Geochemistry, v. 33, p. 1293-1317.

George, S.C., H. Volk, and M. Ahmed, 2007, Geochemical analysis techniques and geological applications of oil-bearing fluid inclusions, with some Australian case studies: Journal of Petroleum Science and Engineering, v. 57, p. 119-138.

Goldstein, R.H., and T.J. Reynolds, 1994, Systematics of fluid inclusions in diagenetic minerals, SEPM Short Course 31: Society of Sedimentary Geology, p. 203

Grimmer, J.O.W., J. Pironon, S. Teinturier, and J. Mutterer, 2003, Recognition and differentiation of gas condensates and other oil types using microthermometry of petroleum inclusions (Abstract): Journal of Geochemical Exploration, v. 78-79, p. 367-371.

Holba, A.G., L.I.P. Dzou, W.D. Masterson, W.B. Hughes, B.J. Huizinga, M.S. Singletary, J.M. Moldowan, M.R. Mello and E. Tegelaar, 1998, Application of 24-norcholestanes for constraining source age of petroleum: Organic Geochemistry, v. 29, p. 1269-1283.

Hughes, W.B., A.G. Holba, and L.I.P. Dzou, 1995, The ratio of dibenzothiophene to phenanthrene and pristane to phytane as indicators of depositional environment and lithology of petroleum source rocks: Geochimica et Cosmochimica Acta, v. 59, p. 3581-3598.

Magyar, I., D.H. Geary, and P. Muller, 1999, Paleogeographic evolution of the Late Miocene Lake Pannon in Central Europe: Palaeogeography Palaeoclimatology Palaeoecology, v. 147, p. 151-167.

Schiefelbein, C.F., J.E. Zumberge, N.R. Cameron, and S.W. Brown, 1999, Petroleum systems in the South Atlantic margins, *in*, N.R. Cameron, R.H. Bate, V.S. Clure (eds.), The oil and gas habitats of the South Atlantic, 153: Geological Society of London Special Publication, p. 169-179.

Schubert, F., L.W. Diamond, and M. Toth, 2007, Fluid-inclusion evidence of petroleum migration through a buried metamorphic dome in the Pannonian Basin, Hungary: Chemical Geology, v. 244, p. 357-381.

Shepherd, T.J., A.H. Rankin, and D.H.L. Alderton, 1985, A Practical Guide to Fluid Inclusion Studies: Blackie and Son Ltd., p. 239.

Sofer, Z., R.D. Regan, and D.S. Muller, 1993, Sterane isomerization ratios of oils as maturity indicators and their use as an exploration tool, Neuquén Basin, Argentina: XII Congreso de Geológico Argentino y II Congreso de Exploración de Hidrocarburos Actas, v. I, p. 407-411.

Szabo, B.M., T. Toth, and F. Schubert, 2009, Paleofluid evolution of the fractured basalt hydrocarbon reservoir in the Üllés-Ruzsa-Bordány area, SE Hungary: Central European Geology, v. 52, p. 299-323.

Tseng, H.Y., and R.J. Pottorf, 2002, Fluid inclusion constraints on petroleum PVT and compositional history of the Greater Alwyn – South Brent petroleum system, northern North Sea: Marine and Petroleum Geology, v. 19, p. 797-809.

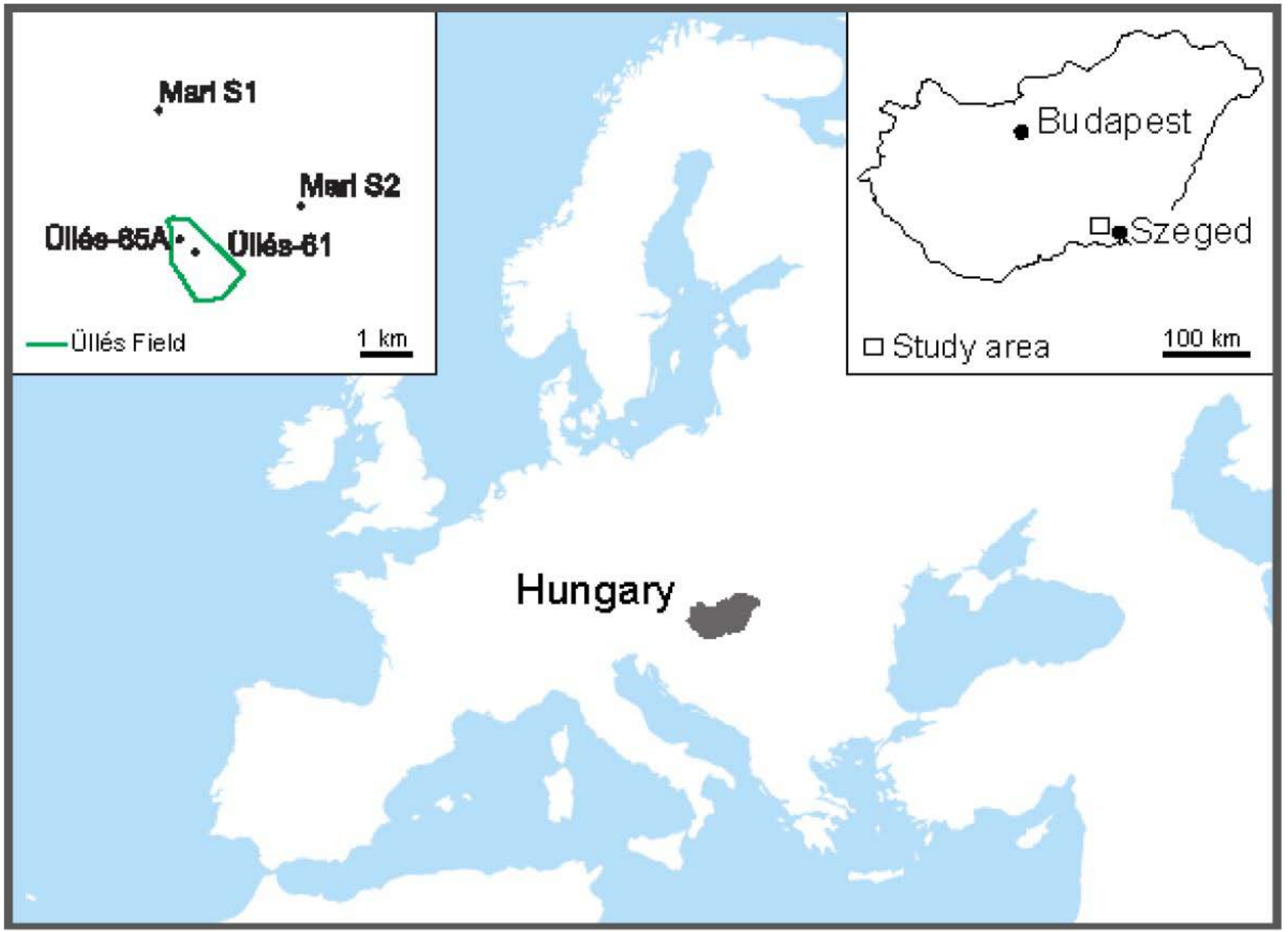

Figure 1. Geographic situation of the study area.

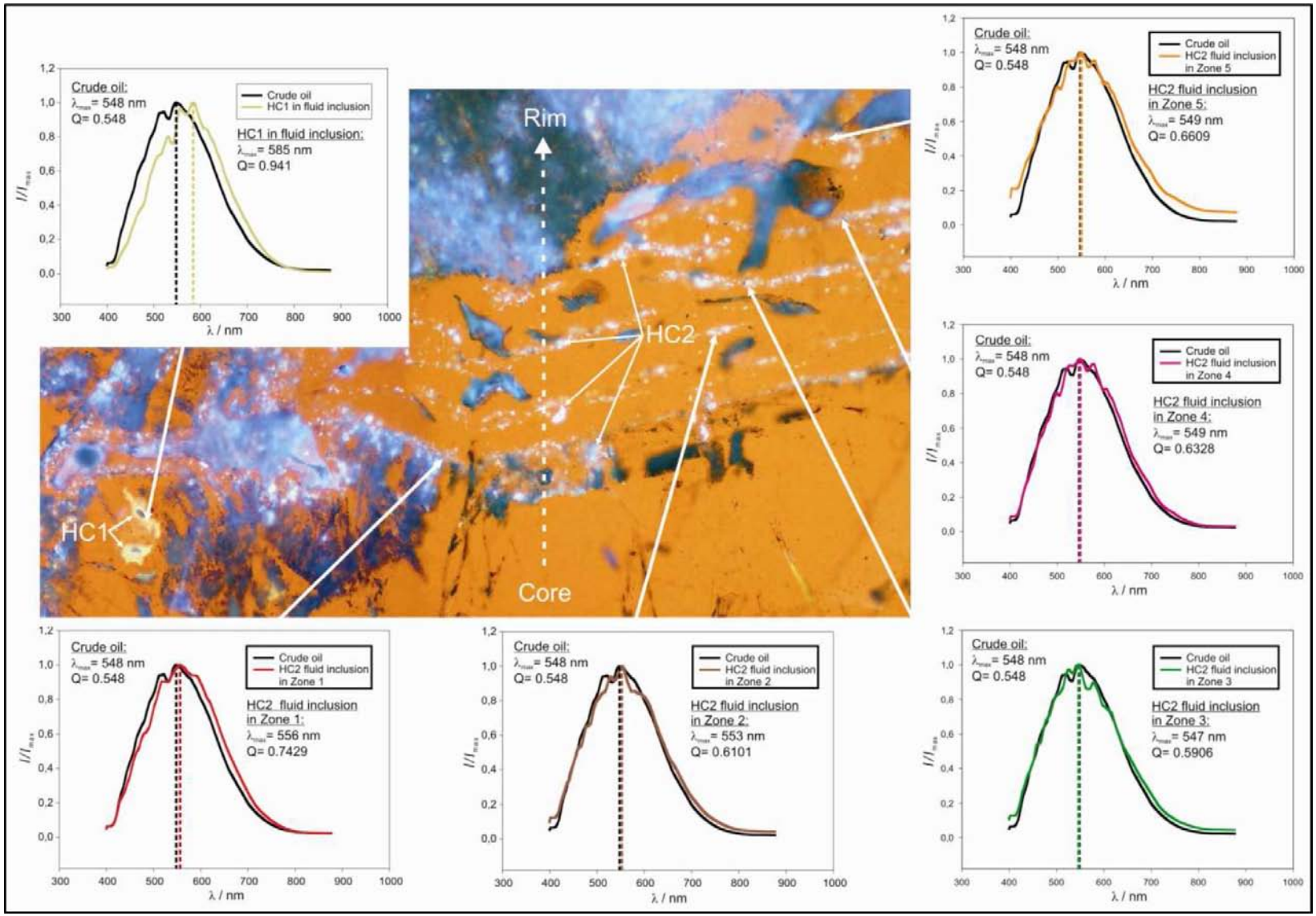

Figure 2. UV fluorescence microspectroscopy profiles of FIOs and crude oil (PO).

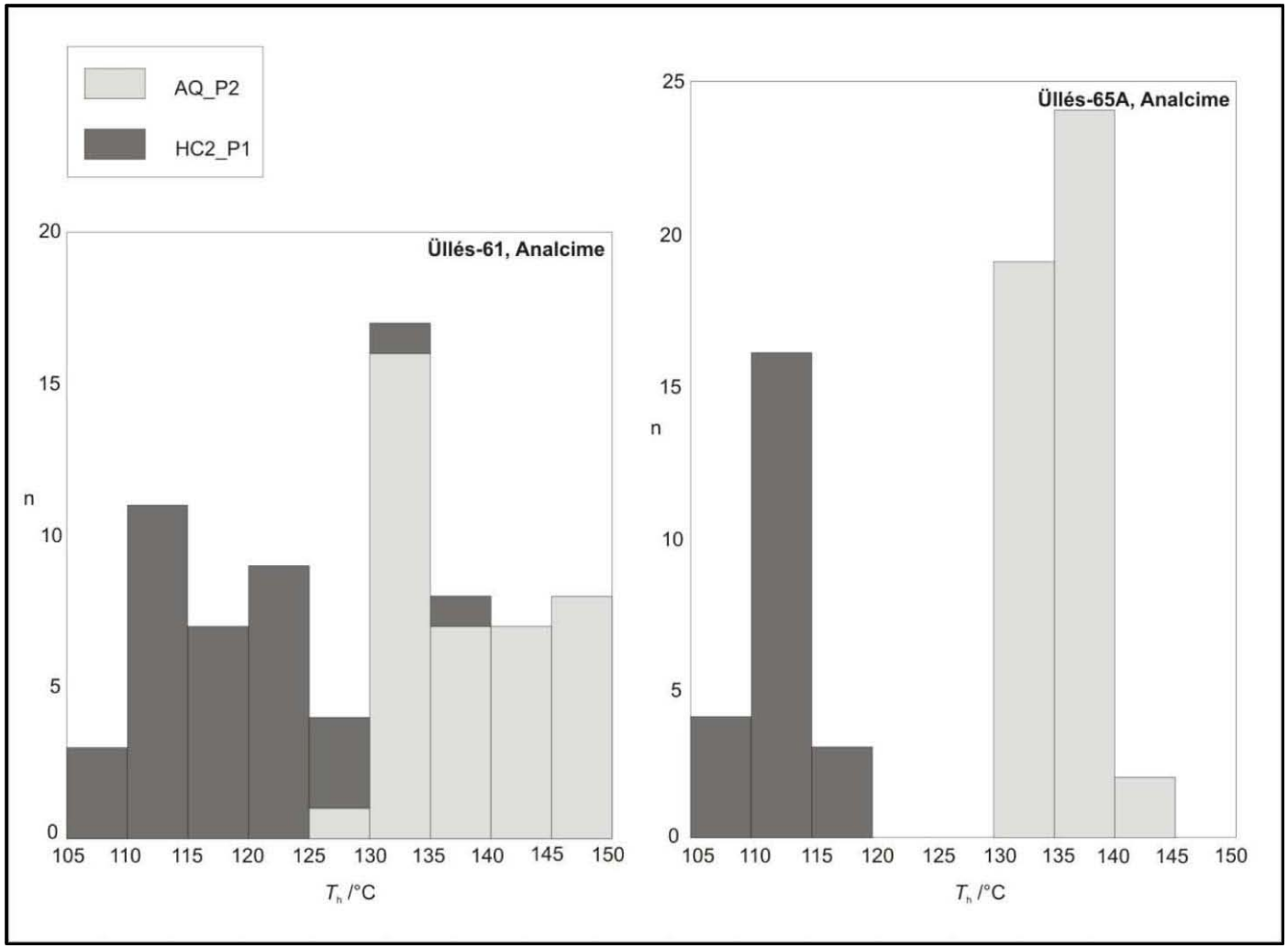

Figure 3. T_h distribution of AQ_P2 and HC2_P1 inclusions in analcime from Ü-61 and Ü65A wells.

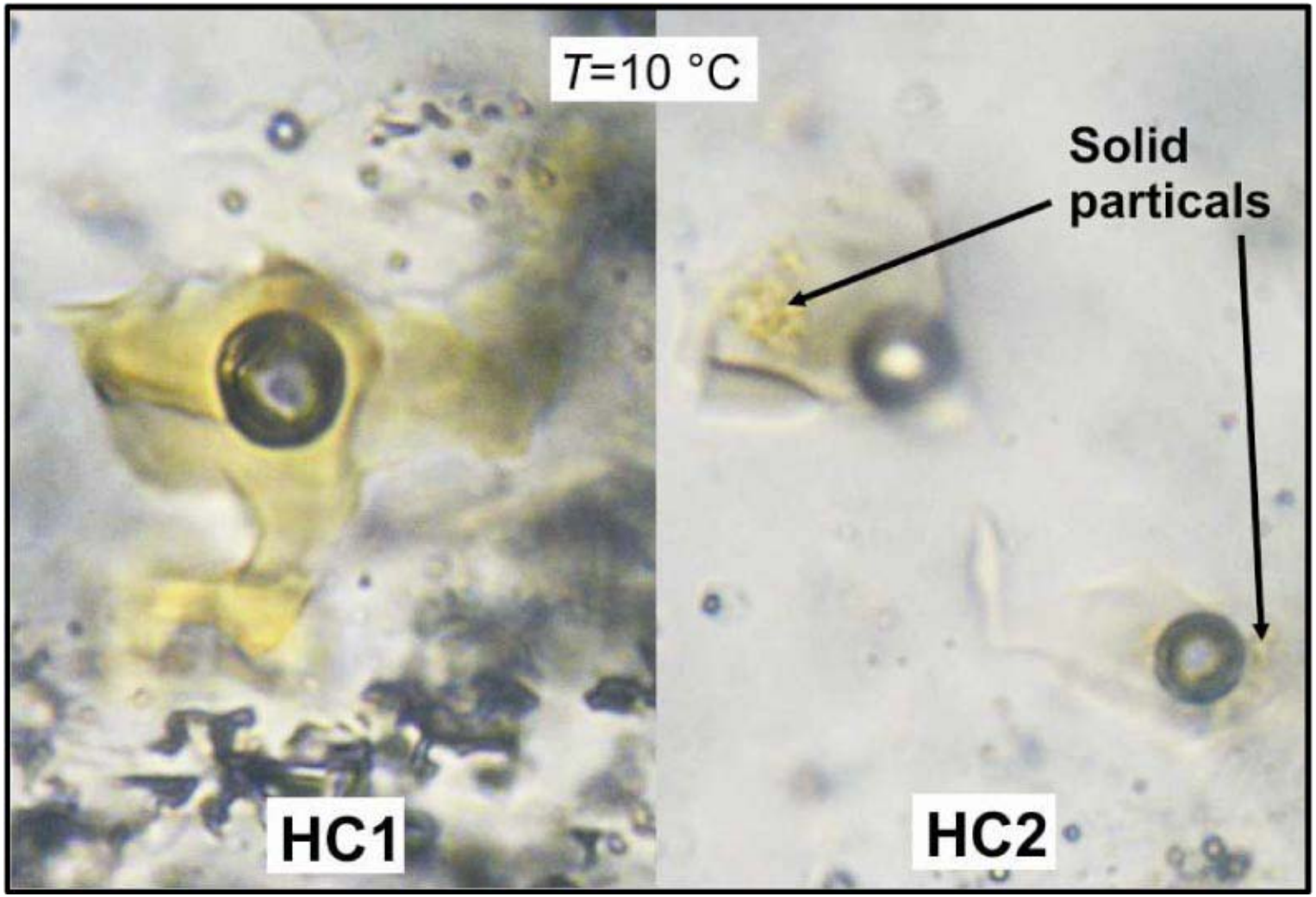

Figure 4. Fluid inclusion petrography on HC containing fluid inclusions at low temperatures.

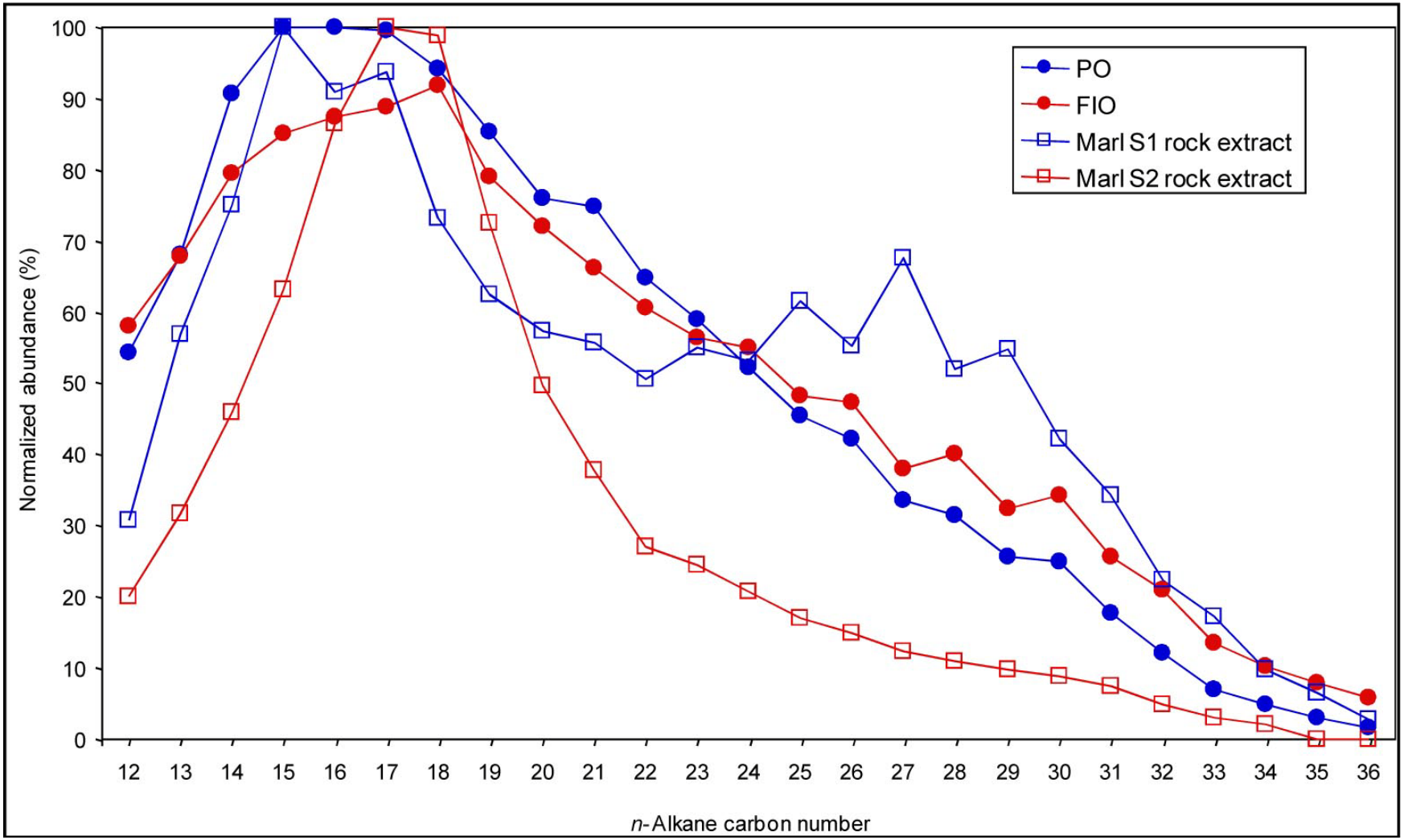

Figure 5. Normalized *n*-alkane envelopes.

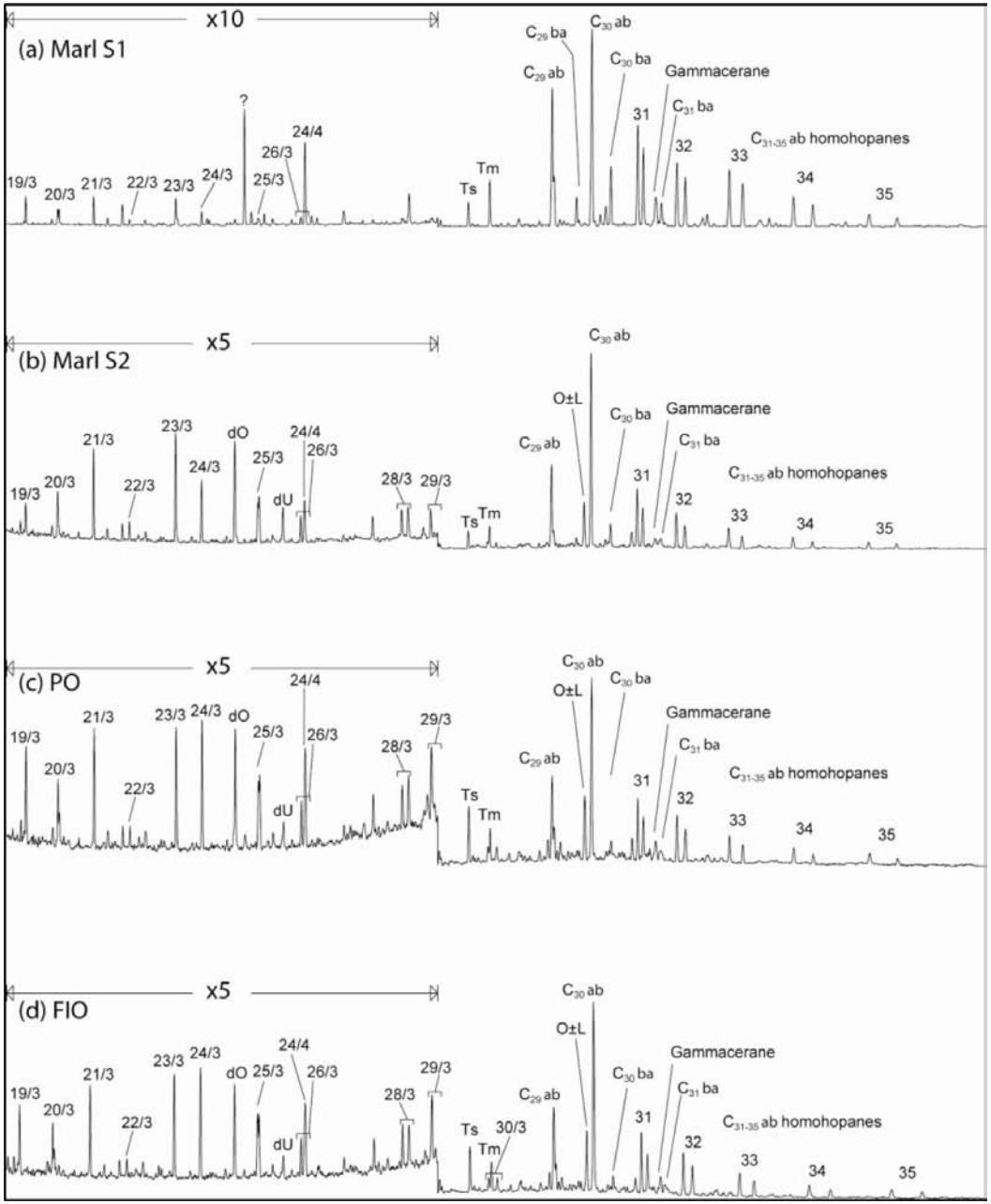

Figure 6. Partial mass chromatograms (*m/z* 191) of the Marl S1 and S2 extracts, and PO and FIO from Üllés 61.

Well, host mineral	Inclusion type	Size (µm)	T_h (℃)	n (number of measurements)	T_m(Ice) (℃)	Salinity m/m%	n
Ü-61, Anl	AQ_P1	2-12	124-145	44	no data	no data	
	AQ_PS	4-20	124-132	16	no data	no data	
	AQ_P2	6-28	129-149	39	-0.3--0.4	0.53-0.71	11
Ü-65A, Anl	AQ_P2	3-66	131-142	45	-0.3	0.53	2
Ü-61, Anl	HC1_P	40	121.5	1			
	HC2_P1	4-8	113-118	35			
	HC2_P2	3-10	110-121	12			
	HC2_P3	3-20	110-121	9			
	HC2_P4	5-11	116-123	5			
	HC2_P5	6-13	111-120	5			
	HC2_S	5-10	113-125	4			
Ü-65A, Anl	HC2_P	3-78	108-118	23			
Ü-61, Heu	HC2_P	8-10	121-134	5			

Table 1. Results of microthermometric measurements.

	Marl S1 extract	Marl S2 extract	U61 PO	U61 FIO	Experiment
Pr/Ph	2.8	1.10	0.67	0.68	SIM
Pr/*n*-C_{17}	0.89	0.76	0.62	0.76	SIM
Ph/*n*-C_{18}	0.40	0.70	0.97	1.09	SIM
CPI (26-32)	1.18	0.99	0.92	0.88	SIM
Ts/Tm	0.55	0.93	2.0	1.6	MRM
C_{30} αβ/(αβ+βα) hopanes	0.88	0.93	0.93	0.94	MRM
C_{35}/(C_{35}+C_{34}) homohopanes	0.33	0.44	0.46	0.44	SIM
C_{29} αβ /C_{30} αβ hopane	0.66	0.44	0.45	0.47	SIM
C_{31} αβ hopanes/C_{30} αβ hopane	0.84	0.58	0.61	0.59	SIM
Homohopanes/C_{30} αβ hopane	2.4	1.50	1.8	1.8	SIM
Oleanane/C_{30} αβ hopane	n.d.	0.25	0.34	0.34	MRM
Gammacerane/C_{30} αβ hopane	0.10	0.03	0.11	0.11	MRM
C_{26} /C_{25} tricyclic terpanes	1.06	0.71	0.67	0.71	SIM
C_{23} tricyclic terpane/C_{30} αβ hopane	0.01	0.10	0.11	0.09	SIM
C_{24} tetracyclic/C_{26} tricyclic terpanes	4.8	0.62	0.94	0.87	SIM
C_{24} tetracyclic/C_{23} tricyclic terpanes	2.4	0.38	0.74	0.77	SIM
C_{19}+C_{20} /C_{23} tricyclic terpanes	1.38	0.72	1.40	1.26	SIM
ETR (Extended Tricyclic Ratio)	n.d.	0.78	0.70	1.00	SIM
C_{29} steranes / C_{29} ab hopanes	0.10	1.25	2.9	2.9	SIM
NDR (24-nor/(24-nor+27-nor) nordiacholestanes	0.49	0.52	0.54	0.58	MRM
NCR (24-nor/(24-nor+27-nor) norcholestanes	0.48	0.56	0.60	0.70	MRM
C_{27} ααα *R* %	36	27	28	28	SIM
C_{28} ααα *R* %	31	38	38	37	SIM
C_{29} ααα *R* %	33	35	34	35	SIM
C_{29}/C_{27} ααα *R*	0.90	1.31	1.25	1.27	SIM
C_{30}/(C_{27}-C_{30}) ααα *R* steranes (%)	n.d.	3.6	3.2	5.5	MRM
$C_{27\text{-}29}$ βα diasteranes / regular steranes	0.26	0.09	0.19	0.19	MRM
C_{29} ααα *S*/(*S*+*R*)	0.41	0.47	0.48	0.49	MRM
VRE from C_{29} *S*/*R* *ααα*	0.70	0.80	0.82	0.84	MRM
C_{29} αββ/(αββ+ααα)	0.47	0.53	0.62	0.63	MRM
C_{27} βα diasterane *S*/(*S*+*R*)	0.59	0.60	0.64	0.61	MRM
TMNr (137TMN/(137+125TMN))	0.41	0.54	0.74	0.71	SIM
TeMNr (1367TeMN/(1367+1256-TeMN))	0.42	0.66	0.83	0.81	SIM
MPI-1 (1.5*(3+2)/(P+9+1)	0.60	0.65	0.65	0.57	SIM
%R_c from MPI-1	0.76	0.79	0.79	0.74	SIM
2-MP/1-MP	0.75	1.08	1.09	1.00	SIM
%R_c from MPR	0.82	0.97	0.98	0.94	SIM
DBT/phenanthrene	0.07	0.08	0.14	0.17	SIM

Table 2. Selected geochemical parameters. For biomarker definitions, see Figure 6.